Polymer Chemistry

ROYAL SOCIETY OF CHEMISTRY

PAPER

View Article Online
View Journal | View Issue

Cite this: *Polym. Chem.*, 2023, **14**, 284

A self-crosslinking nanogel scaffold for enhanced catalytic efficiency and stability†

Xu Yang,‡[b] Maosheng Lin,‡[b] Jirui Wei[b] and Jing Sun *[a]

Received 6th October 2022,
Accepted 27th November 2022

DOI: 10.1039/d2py01272c

rsc.li/polymers

We report the preparation of a series of polypeptoid derivatives with different side-chain functionalities by sequential photocleavage and thiol–ene reactions with high efficiency. In particular, thermo-responsive *N*-isopropylacrylamide (NIPAM) motifs were grafted onto polypeptoids to achieve the lower critical solution temperature (LCST) property. The incorporation of allyl groups to a block copolymer poly(ethylene glycol)-*b*-poly(*N*-(S-(*o*-nitrobenzyl)-thioethyl)glycine)-*co*-poly(*N*-allyl glycine) (PEG-*b*-PNSN-*co*-PNAG) enables the preparation of UV-initiated self-crosslinking nanogels for further immobilization of lipase and gold nanoparticles in aqueous solution. The obtained hybrid nanogels exhibit significantly enhanced catalytic efficiency and adjustable bioactivity as compared to the free lipase and gold nanoparticles. The hybrid nanogel showed a significantly higher conversion value of >200% compared to native lipase. By incorporating the NIPAM motifs, thermoresponsive hybrid nanogels have been fabricated and 89.8% of the residual enzymatic activities are retained at 50 °C. This work provides a facile and efficient approach to prepare multifunctional bioinspired platforms under mild conditions that offer increased catalytic efficiency and stability.

Introduction

Stimuli-responsive polymers are a class of smart materials that can vary their chemical structure or physical properties under external stimuli (such as light, temperature, pH, *etc.*). Due to their advantageous properties, stimulus-responsive polymers have been widely used in nanotechnology and nanomedicine.[1–8] In particular, light has attracted great attention because of its excellent controllability in time and space.[9–15] The versatile *o*-nitrobenzyl derivatives are one of the most studied photoresponsive motifs for many applications.[11,16] In most studies, carboxylic acids and amines are produced through photolysis of the polymers bearing *o*-nitrobenzyl groups.[17–20] However, highly reactive thiols have rarely been reported due to the synthetic challenge.[21–27] It is known that the thiol–ene chemistry is typically used as a potent tool for versatile polymer modification.[28] Thus, the produced thiols offer great advantages to obtain various polymeric materials with highly designable functionalities. Lately, nanogels formed from cross-linking of polymer materials have emerged as nano-scale polymer networks, and have attracted increasing attention.[29] Smart nanogels prepared from stimuli-responsive polymers are endowed with improved multifunctional properties for a variety of applications.[30–34] These nanogels can be employed to load drugs, catalysts, and biomolecules as stimuli-responsive nanocarriers.[35–39] The delicate design of polymers to construct smart nanogels is desired.

Polypeptoids are a type of bioinspired polymer material possessing an identical backbone of polyglycine with *N*-substituted side chains, and exhibit good biocompatibility and biological activities.[40–45] The properties of polypeptoids are highly tunable, and are determined by the side-chain moiety because of the absence of the hydrogen bond and chirality on the backbone. Polypeptoids bearing alkyl side chains have been extensively studied, and can be readily synthesized *via* ring-opening polymerization (ROP). In contrast, the preparation of polypeptoids with versatile functionalities is limited, where the protecting chemistry is typically required. A couple of stimuli-responsive polypeptoids with pH-, photo- and temperature-responsive functionalities *via* ring-opening polymerization (ROP) and post-polymerization modification have been reported.[46–50] We have previously prepared a type of photoresponsive polypeptoid that forms reversible self-crosslinking assemblies by disulfide–thiol chemistry upon UV-irradiation.[51] Herein, we prepared a class of photoresponsive homopolypeptoid poly(*N*-(S-(*o*-nitrobenzyl)-thioethyl)glycine) (PNSN) and its block copolymer poly(ethylene glycol)-*b*-poly(*N*-(S-(*o*-nitrobenzyl)-thioethyl)glycine) (PEG-*b*-PNSN), which offer efficient platforms for versatile functionalities. In addition, the incorporation of allyl groups into the system generates a new type of

[a]*State Key Laboratory of Supramolecular Structure and Materials, College of Chemistry, Jilin University, Changchun 130012, China. E-mail: jingsun@jlu.edu.cn*
[b]*Key Laboratory of Biobased Polymer Materials, College of Polymer Science and Engineering, Qingdao University of Science and Technology, Qingdao 266042, China*
†Electronic supplementary information (ESI) available. See DOI: https://doi.org/10.1039/d2py01272c
‡These authors contributed equally.

self-crosslinking nanogel initiated by UV light in aqueous solution in one-pot synthesis, which offers great potential for immobilization of lipase and a nanoreactor containing gold nanoparticles with superior properties.

Experimental

Materials and instruments

Hexane, tetrahydrofuran (THF), and dichloromethane (DCM) were purified by purging with dry nitrogen, followed by passing through columns of activated alumina. *N*,*N*-Dimethylformamide (DMF) was treated with a free amine scavenger (Aldrich, Berlin, Germany) before passing through 4 Å molecular sieves and an activated alumina column. Ethyl acetate (EtOAc) was freshly distilled from CaH_2. Methoxypolyethylene glycol amine (mPEG-NH_2, M_w = 2000 g mol^{-1}) was purchased from Jenkem Technology Co, Ltd (Beijing, China). *o*-Nitrobenzyl bromide was purchased from Ark Pharm Reagent Co., Ltd (Chicago, IL, USA). Cysteamine hydrochloride (98%) and 4-nitrophenyl palmitate (*p*NPP) were purchased from Adamas Reagent Co., Ltd (Shanghai, China). Allylamine, hexylamine, di-*tert*-butyl dicarbonate, and glyoxylic acid monohydrate were purchased from Titan Reagent (Shanghai, China). Phosphorus trichloride and triethylamine were purchased from Sinopharm Chemical Reagent Co., Ltd. *N*-Isopropylacrylamide (NIPAM), acrylamide, acrylonitrile, *N*-ethyl maleimide, *N*-benzyl maleimide, 2-hydroxy-4′-(2-hydroxyethoxy)-2-methylpropiophenone (I_{2959}) and 2,2-dimethoxy-2-phenylacetophenone (DMPA) were purchased from Aladdin Bio-Chem Technology. Lipase and 2-iminothiolane hydrochloride (Traut's reagent) were purchased from Macklin Biochemical Co. Ltd. All other chemicals were purchased from commercial suppliers and used without further purification unless otherwise noted.

^{1}H NMR spectra were recorded on a Bruker AV400 FT-NMR spectrometer. Gel permeation chromatography/laser light scattering (GPC/LLS) was performed at 50 °C using an SSI (Series I) pump (LC20AT, Shimadzu Corporation, Kyoto, Japan) connected to a Wyatt Optilab DSP with 0.05 M LiBr in DMF as the eluent at a flow rate of 1.0 mL min^{-1}. Conventional calibrations were performed using polystyrene standards (PS). Transmission electron microscopy (TEM) samples were examined using a JEM2200FS transmission electron microscope (200 keV, Tokyo, Japan). TEM samples were prepared by pipetting the polymer solution on carbon coated TEM grids and an excess amount of the polymer solution was blotted with a piece of filter paper. The hydrodynamic diameter (D_h) of the assemblies was determined at 25 °C by dynamic light scattering (DLS) using a Brookhaven NanoBrook instrument (Holtsville, NY, USA). The CP, defined as the temperature corresponding to 50% transmittance during the heating process, was measured by monitoring the transmittance of a 500 nm light beam through a quartz sample cell at a concentration of 2 mg mL^{-1} on a Shimadzu UV-vis spectrometer (Shimadzu, Japan). The sample was irradiated using a mercury high-pressure UV lamp (250 W, GGZ250, Shanghai Jiguang Special Lighting Electrical Factory, Shanghai, China). The gold ion concentration was measured using an inductively coupled plasma optical emission spectrometer (ICP-OES) (PerkinElmer, Avio200). The samples were stored avoiding exposure to light.

Synthesis of the poly(*N*-(S-(*o*-nitrobenzyl)-thioethyl)glycine) (PNSN)

The *N*-(S-(*o*-nitrobenzyl)-thioethyl)-*N*-carboxyanhydride (NSN–NCA) monomer was synthesized according to the previous work.[47,51,52] The solution of NSN–NCA (100 mg mL^{-1} in anhydrous THF) was then added to the polymerization tube, followed by the addition of a stock solution of hexylamine (1.5 wt% in THF). The polymerization was performed under a N_2 atmosphere at 55 °C and monitored by FTIR spectroscopy until the disappearance of the characteristic peaks (1850 and 1790 cm^{-1}) of NCAs. The final solution was precipitated into excess cold diethyl ether. The product was dried under reduced pressure to yield a yellow solid (62.5% yield). ^{1}H NMR (400 MHz, chloroform-d) δ: 7.89 (d, 7H), 7.28–7.63 (m, 21H), 3.80–4.53 (s, 28H), 3.28–3.67 (t, 14H), 3.06–3.27 (*t*, 2H), 2.43–2.86 (*t*, 14H), 1.14–1.51 (m, 8H), 0.83 (t, 3H).

Synthesis of the poly(ethylene glycol)-*b*-poly(*N*-(S-(*o*-nitrobenzyl)-thioethyl)glycine) block copolymer (PEG-*b*-PNSN)

mPEG-NH_2 was completely dried under vacuum for 30 h and dissolved in anhydrous THF in a polymerization tube, followed by the addition of a given ratio of the NSN–NCA solution (100 mg mL^{-1} in THF). After stirring at 55 °C for 48 h, the mixed solution was precipitated into excess diethyl ether. The product was dried under vacuum at 30 °C. A pale yellow oil was obtained (60% yield). ^{1}H NMR (400 MHz, chloroform-d) δ: 7.81–8.01 (d, 10H), 7.29–7.61 (m, 30H), 3.86–4.42 (s, 40H), 3.59–3.69 (m, 176H), 3.34–3.52 (t, 20H), 3.38 (s, 3H), 2.46–2.85 (t, 20H).

Synthesis of the poly(ethylene glycol)-*b*-poly(*N*-(S-(*o*-nitrobenzyl)-thioethyl)glycine)-*co*-poly(*N*-allyl glycine) (PEG-*b*-PNSN-*co*-PNAG)

The mixtures of *N*-(S-(*o*-nitrobenzyl)-thioethyl)-*N*-carboxyanhydride (NSN–NCA) (100 mg mL^{-1}) and *N*-allyl *N*-carboxyanhydride (NAG-NCA) (120 mg mL^{-1}) in anhydrous THF with mPEG-NH_2 as the initiator were added in a polymerization tube. The solution was stirred at 55 °C for 48 h under nitrogen, and the polymerization progress was monitored by FTIR. The solution was precipitated into an excess of cold diethyl ether. A pale yellow oil was collected by centrifugation, washed three times with cold diethyl ether and dried under reduced pressure to yield a yellow oil (56% yield). ^{1}H NMR (400 MHz, chloroform-d) δ: 7.87–8.02 (d, 10H), 7.32–7.64 (m, 30H), 5.59–5.94 (m, 25H), 5.01–5.35 (d, 50H), 3.84–4.36 (m, 140H), 3.59–3.69 (m, 176H), 3.39–3.53 (t, 20H), 3.38 (s, 3H), 2.50–2.80 (t, 20H).

Preparation of the polypeptoid derivatives

PEG-*b*-PNSN (100 mg, 0.022 mmol) was first dissolved in 5 mL of anhydrous DMF in a 25 mL Schlenk flask. The flask was degassed by freeze–pump–thaw cycles three times and purged

with N_2 for 15 min. The solution was then irradiated with mercury high-pressure UV light for 5 h under stirring. After this, 250.3 mg of NIPAM (2.212 mmol, 10 equivalents of [NSN]) and 5.6 mg of DMPA (0.022 mmol, 1 equivalent of [NSN]) were added under a nitrogen atmosphere, and the irradiation was continued for another 5 h. After the reaction, the mixture solution was placed in a dialysis bag (MWCO = 3500), and first dialyzed with DMF for 48 h, followed by dialysis with deionized water for 24 h. Finally, the aqueous solution was freeze-dried to obtain a pale yellow powder (85 mg, 85% yield). ^{1}H NMR (400 MHz, DMSO-*d*) δ: 7.81–8.01 (d, 5H), 7.29–7.61 (m, 15H), 7.20 (s, 5H), 3.71–4.16 (m, 35H), 3.59–3.69 (m, 176H), 3.34–3.52 (t, 20H), 3.38 (s, 3H), 2.46–2.85 (t, 20H), 1.78–2.21 (t, 10H), 1.33–1.68 (t, 10H), 0.98–1.09 (d, 30H).

All the other polypeptoid derivatives were obtained in a similar way. In the case of PEG-*b*-PNSN-*co*-PNAG co-polypeptoids, DMPA was added for chemical cross-linking.

Preparation of the PEG-*b*-PNSN-*co*-PNAG nanogel aqueous solution

10 mg of freeze-dried PEG-*b*-PNSN-*co*-PNAG after irradiation was added into 3 mL of DMF and placed in a dialysis bag (MWCO = 3500), followed by dialysis with deionized water for 24 hours. The concentration of the aqueous solution was fixed at 1 mg mL^{-1} for further measurement.

The preparation of the non-irradiated micellar solution was similar to the above method, except that exposure of the solutions to natural light was avoided in the entire procedure.

Preparation of the hybrid nanogel-immobilized with lipase

Before conjugation with nanogel, lipase was modified with thiol groups by using Traut's reagent. A typical procedure for the synthesis of thiol-modified lipase is as follows.[53] Native lipase (40 mg) was dissolved in 10 mL of PBS buffer (pH = 8.0, 0.1 M) in a Schlenk flask. This flask was purged with nitrogen gas flow for more than 30 min. Traut's reagent (1 mg) was added to the solution. The reaction was conducted in an oil bath at 30 °C for 60 min.

10 mL (2 mg mL^{-1}) of nonirradiated PEG-*b*-PNSN-*co*-PNAG micelle solution (PBS buffer, pH = 8.0) was placed in a Schlenk flask and bubbled with nitrogen for 30 min. After 6 h of UV-irradiation, 10 mL of thiol-modified lipase solution (4 mg mL^{-1}) and the water-soluble initiator I_{2959} were added under a nitrogen atmosphere. The flask was exposed to UV-irradiation for another 3 h under continuous magnetic stirring. After the reaction, the conjugates were purified by performing centrifugation/washing cycles (9000 rpm, 10 min) for the removal of free lipase. The upper solution containing free lipase was removed and the covalent conjugates were re-dispersed in PBS buffer. The mixture solution was then dialyzed (MWCO = 25 000) against PBS buffer for 48 h in an ice bath and stored at 2 °C. The final concentration of the lipase in the obtained mixture solution was determined using a UV-vis spectrometer.

The preparation method of the lipase-containing nanogels modified with *N*-isopropylacrylamide (NIPAM) is similar to the above method.

Lipase activity assay

4-Nitrophenyl palmitate (*p*NPP) was selected as a substrate for the bioactivity study. The catalytic capacities of native lipase and the hybrid nanogels were determined by the absorbance of the hydrolysis product of *p*-nitrophenol on a UV-vis spectrometer at 37 °C. 2 mL of native lipase solution or hybrid nanogel solution containing the same amount of lipase was mixed with 40 μL of substrate solution (4 mg mL^{-1} in acetonitrile), respectively. The absorbance of the solution at λ = 400 nm was constantly measured for each sample for evaluating the catalytic capacity. The residual enzymatic activities at different temperatures were carried out by the following procedure. Prior to the addition of *p*NPP, the hybrid nanogel and the free lipase solution were incubated at a designated temperature for 30 minutes. The absorbance was then measured at 37 °C. The residual enzymatic activities were assayed and compared with those measured at 37 °C.

Preparation of the polypeptoid–AuNP hybrid nanogels

410 μL of $HAuCl_4$ aqueous solution (1 mg mL^{-1}) and the photoinitiator I_{2959} (5 mg) were added into the nonirradiated PEG-*b*-PNSN-*co*-PNAG micelle solution (5 mL, 1 mg mL^{-1}). After stirring for 30 min, the mixed solution was exposed to UV-irradiation for 5 h. The mixed solution was then dialyzed against DI water to remove by-products and free AuNPs. The absorption spectrum of the obtained AuNP-containing hybrid nanogels (nanogels@Au) was recorded using a UV-vis spectrometer. The concentration of Au in the hybrid nanogel solution was found to be 28.08 μg mL^{-1} using an inductively coupled plasma optical emission spectrometer.

The AuNPs were prepared by a typical seed synthesis method as previously reported.[54]

Reduction of *p*-NP catalyzed by polypeptoid–AuNP hybrid nanogels

The catalytic reduction of *p*-NP was carried out in a quartz cuvette in the presence of the catalyst (nanogels@Au) and $NaBH_4$. As a control, both the nanogels and AuNPs were used. In a typical process, the stock solutions of *p*-NP (10 μL, 0.01 M) and $NaBH_4$ (133 μL, 0.1 M) were added into 1.86 mL of hybrid nanogel solution or the free AuNP solution in the quartz cuvette. The reaction was monitored at 400 nm using a UV-vis spectrometer at different time intervals.

Results and discussion

Synthesis of the photoresponsive polypeptoid-based copolymers

The *N*-(S-(*o*-nitrobenzyl)-thioethyl)-*N*-carboxyanhydride (NSN–NCA) and *N*-allyl *N*-carboxyanhydride (NAG-NCA) monomers were synthesized following the reported methods (Scheme S1†).[47,51] The chemical structures of both monomers were confirmed by ^{1}H NMR spectroscopy (Fig. S1†). The homopolymer PNSN and the copolymers PEG-*b*-PNSN and PEG-*b*-PNSN-*co*-PNAG were synthesized *via* ROP of the NSN–NCA monomer or mixtures of NSN–NCA and NAG-NCA with the nucleophilic initiator hexylamine and the macroinitiator

mPEG-NH_2 (Schemes S2 and S3a†), respectively. The disappearance of the two characteristic $\nu_{C=O}$ peaks at 1780 cm^{-1} and 1850 cm^{-1} of the monomer suggests complete conversion of the NCA monomer by FTIR (Fig. S2†).[55–57] The ^{1}H NMR spectra show that all the peaks of the synthesized copolymer are well assigned, confirming their chemical structures (Fig. 1a, 2a and 3a). A series of copolymers with different degrees of polymerization (DPs) were further synthesized by varying the ratio of NCAs to the initiators. All the molecular characteristics of the photoresponsive polypeptoid copolymers are shown in Table 1. The subscript numbers represent the DPs of the blocks. The GPC traces show narrow molecular weight distributions with dispersity ($Đ$) ≤1.26, indicating the well-controlled polymerization in all cases (Fig. S3†).

Synthesis of the polypeptoid derivatives

In order to investigate the grafting efficiency of the photoresponsive polypeptoids, the homopolymer PNSN and the diblock copolymer PEG-*b*-PNSN were used as the polymer precursors (Scheme S4†). Three commercially available allyl-containing compounds (*N*-isopropylacrylamide, acrylamide and acrylonitrile) and two maleimide-containing compounds (*N*-ethyl maleimide and *N*-benzyl maleimide) were used for side-chain modification *via* the sequential photocleavage reaction and thiol–ene click reaction (Scheme 1a).

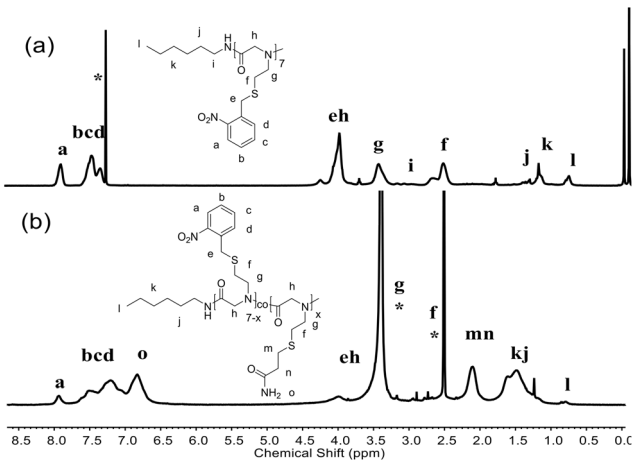

Fig. 1 ^{1}H NMR spectra of PNSN (a) in $CDCl_3$ and the block co-polypeptoid **1b** (b) in DMSO. * indicates solvents.

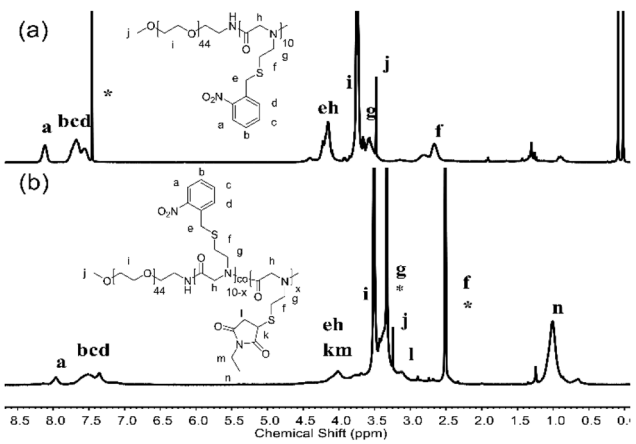

Fig. 2 ^{1}H NMR spectra of (a) PEG-*b*-PNSN in $CDCl_3$ and (b) **2d** in DMSO. * indicates solvents.

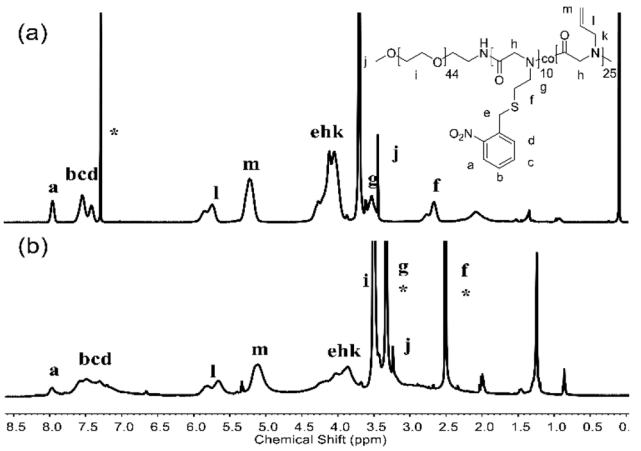

Fig. 3 ^{1}H NMR spectra of PEG-*b*-PNSN-*co*-PNAG in $CDCl_3$ (a) with 10-h irradiation (b) in DMSO. * indicates solvents.

In all cases, 2,2-dimethoxy-2-phenylacetophenone (DMPA) was used as an efficient photocatalyst for the thiol–ene reaction according to the previous reports.[17,47] The post-modification reactions were performed in two sequential steps, in which the modification step was applied after the photocleavage step, which can avoid the potential side reactions during photolysis (Scheme S4†). We obtained a series of polypeptoids modified with five types of functional side-chain groups. In contrast to the photocleavage ratio ranging from 50% to 80%, nearly all products are quantitatively modified with a grafting ratio of 100%, which indicates the high efficiency of the side chain modification of polymers (Table 2). In a typical procedure, PNSN was modified with acrylamide to yield **1b**, where the protons of the newly formed CH_2SCH_2 bond at δ ~1.93–2.26 ppm can be observed by ^{1}H NMR (Fig. 1b). In addition, the appearance of the proton of $-NH_2$ at δ ~6.61–6.99 ppm and the decreased peaks of the *o*-nitrobenzyl (NB) group at δ ~7.29–8.01 ppm are also visible.[51,52] The photocleavage ratio was obtained by comparing the proton integral ratio of "a" before and after the irradiation, and the grafting rate was calculated by considering the integral ratio of "m, n" and the photolysis proton "a" (Fig. 1). It is generally accepted that the thiol–maleimide reaction shows high efficiency, which may result in a 100% grafting ratio.[22] Note that quantitative grafting also occurred in acrylonitrile modification of PNSN. Furthermore, the diblock copolymer PEG-*b*-PNSN was conjugated with *N*-ethyl maleimide to obtain **2d**. The chemical structure of **2d** was confirmed by ^{1}H NMR, as shown in Fig. 2b. A newly formed characteristic peak of $-CH_3$ at δ ~0.78–1.12 ppm of *N*-ethyl maleimide was observed in the ^{1}H NMR spectra, confirming the successful modification.

Table 1 Characteristics of the synthesized polymers

Samples	Feed ratio[a]	Gain ratio[b]	M_n [b] (kDa)	M_n [c] (kDa)	Dispersity ($Đ$)[c]
$PNSN_7$	1/10	1/7	1892	4035	1.26
PEG_{44}-*b*-$PNSN_{10}$	1/10	1/10	4560	7269	1.20
PEG_{44}-*b*-$PNSN_{10}$-*co*-$PNAG_{25}$	1/10/20	1/10/25	6985	11 080	1.18
PEG_{44}-*b*-$PNSN_{20}$-*co*-$PNAG_{40}$	1/20/40	1/20/40	10 920	15 040	1.12

[a] Feed molar ratio of initiator/NSN–NCA/allyl-NCA. [b] Calculated from the ^{1}H NMR spectra. [c] Determined from gel permeation chromatography (GPC).

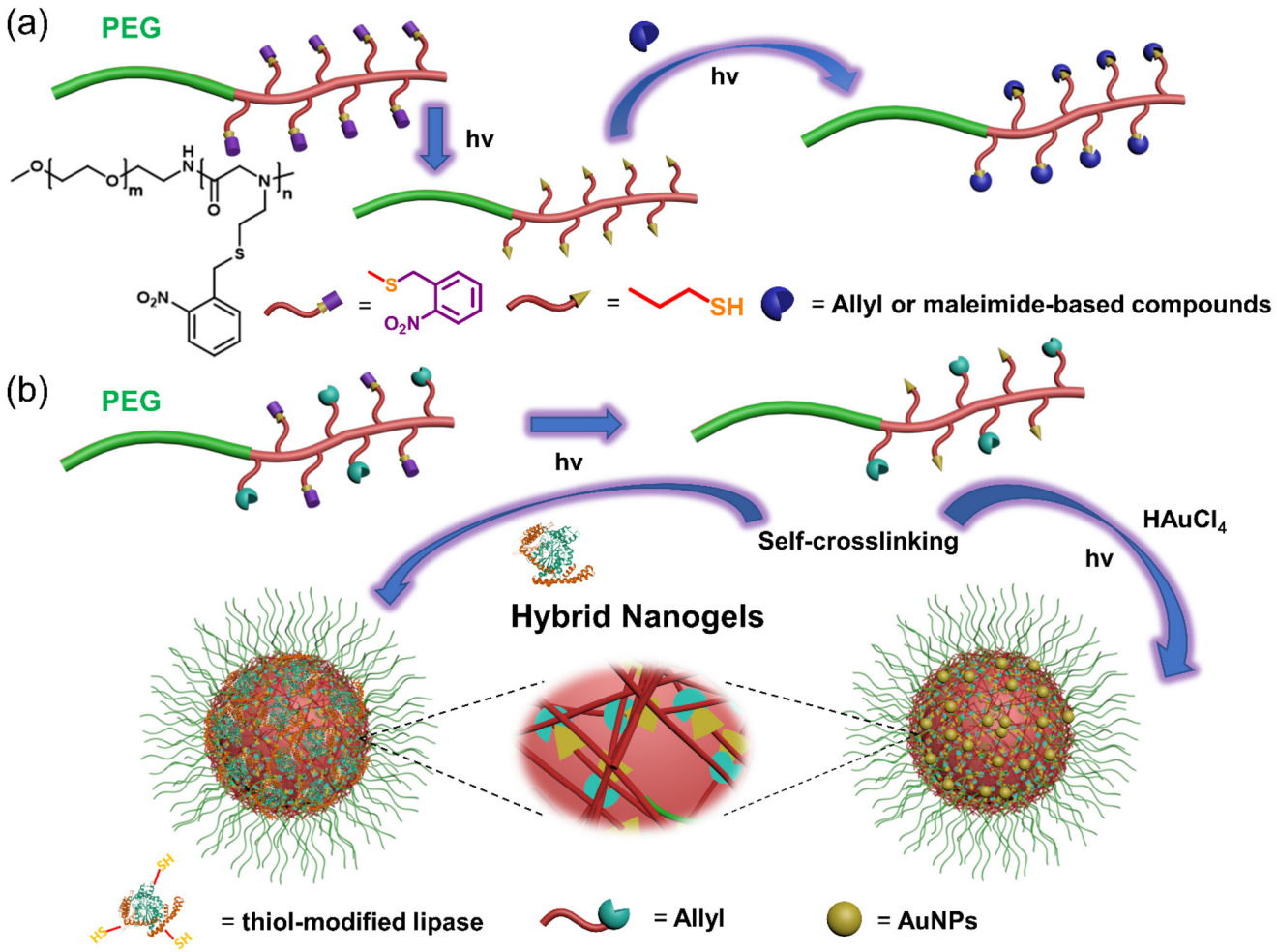

Scheme 1 (a) Side chain modification of photoresponsive polypeptoid copolymers. (b) Schematic graph of self-crosslinking nanogels from photoresponsive polypeptoid copolymers.

The characteristics of polypeptoid copolymers modified with different compounds are shown in Table 2. The related ^{1}H NMR spectra are shown in the ESI (Fig. S4 and S5†). In all cases, the grafting ratios are as high as 100% irrespective of the species of the compounds. In comparison with the homopolypeptoid, the diblock copolymer containing PEG shows enhanced grafting efficiency, which is possibly because the solubility is increased by incorporating the PEG block.

In addition, we designed a type of block copolymer poly(ethylene glycol)-*b*-poly(*N*-(S-(*o*-nitrobenzyl)-thioethyl)glycine)-*co*-poly(*N*-allyl glycine) (PEG-*b*-PNSN-*co*-PNAG) that contains a random co-polypeptoid PNSN-*co*-PNAG block. By the incorporation of PNAG residues on the side chain, a photoinitiated self-crosslinked system was constructed (Scheme 1 and S3†). As shown in Fig. 3b, upon UV-irradiation, photocleavage of the NB group occurs accompanied by decreased peaks of –CH=CH_2 groups at δ ~5.12–5.83 ppm and NB groups at δ ~7.29–8.01 ppm. This suggests the occurrence of the self-crosslinking of polymer chains *via* a thiol–ene click reaction, which is further confirmed by GPC (Fig. S6†). Considering the con-

Table 2 Synthesis of the polypeptoid polymers with different side groups

Entry	Modified side chain group	Photocleavage ratio[a] (mol%)	Grafting ratio[a] (mol%)
PNSN	—	—	—
1a	*N*-Isopropylacrylamide	85	83
1b	Acrylamide	57	75
1c	Acrylonitrile	71	100
1d	*N*-Ethyl maleimide	71	100
1e	*N*-Benzyl maleimide	85	100
PEG-*b*-PNSN	—	—	—
2a	*N*-Isopropylacrylamide	50	100
2b	Acrylamide	50	100
2c	Acrylonitrile	50	100
2d	*N*-Ethyl maleimide	60	100
2e	*N*-Benzyl maleimide	60	100
PEG-*b*-$PNSN_{10}$-*co*-$PNAG_{25}$	—	50	100
PEG-*b*-$PNSN_{20}$-*co*-$PNAG_{40}$	—	60	100

[a] Both the photocleavage ratio of NB groups for PNSN blocks and the grafting ratio of the modified side chain groups were calculated from the ^{1}H NMR spectra.

centration, it is likely that the crosslinking occurs in both intra- and inter-polymer chains. The GPC analysis shows that the PEG-*b*-PNSN-*co*-PNAG copolymer upon 10 h of irradiation exhibits two distributions, where one peak is similar to that of the non-irradiated sample and the other major peak shifts to a significantly higher molecular weight with a broad distribution. This further confirms the successful interchain self-crosslinking.

The solution property of the modified polypeptoids

Poly(*N*-isopropylacrylamide) is a typical thermoresponsive polymer with a reversible phase transition of the lower critical solution temperature (LCST).[58] The *N*-isopropylacrylamide moieties were grafted onto the polypeptoids to yield **1a** and **2a** (Fig. S3a and S4a†). PEG-*b*-PNSN modified with *N*-isopropylacrylamide (**2a**) can readily dissolve in aqueous solution. As expected, the obtained polymers show thermoresponsive behavior in aqueous solution, where a reversible LCST phase transition of the solution from clear to cloudy upon heating occurs as the temperature increases to 35 °C (Fig. 4a). In addition, after 5 heating and cooling cycles between 20 and 60 °C, the phase transition is recovered, indicating good stability of the polymer solution (Fig. 4b). In the case of **1a**, a suspension rather than a clear aqueous solution is present at room temperature, possibly due to the limited solubility (Fig. S7†). Nevertheless, the variations of the transmittance during the heating and cooling process are still visible. We further synthesized polypeptoids modified with acrylamide and acrylonitrile motifs to yield **1b**, **1c**, **2b** and **2c**. Unfortunately, due to the hydrophobicity of the nitrile groups, the obtained **1c** and **2c** are difficult to disperse in aqueous solution. Instead, the samples modified with acrylamide groups have good water solubility.

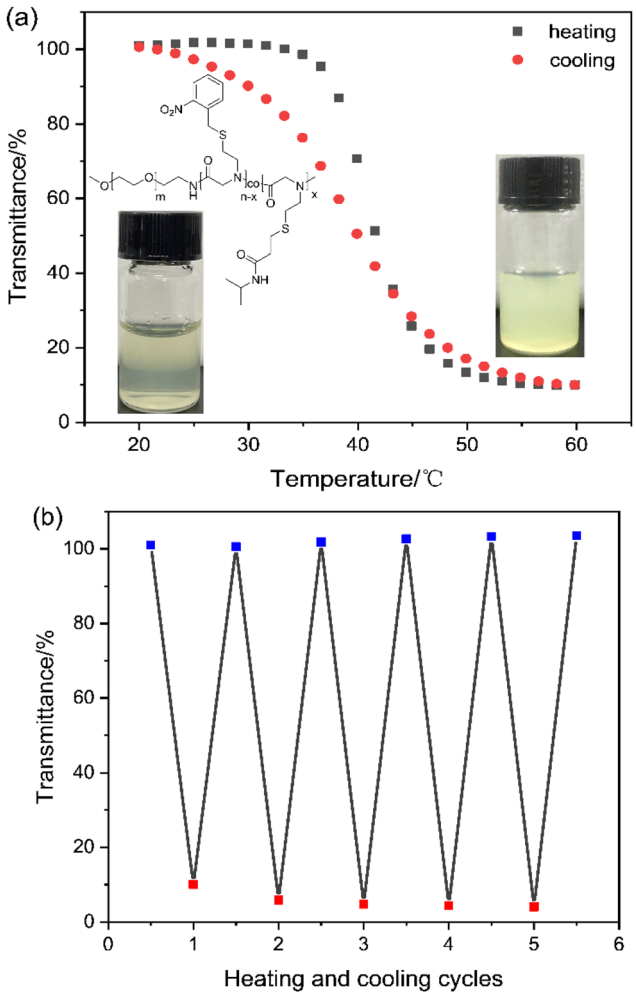

Fig. 4 (a) Plots of transmittance as a function of temperature for aqueous solutions (2 mg mL^{-1}) of **2a**. (b) Transmittance of **2a** aqueous solution at a concentration of 2 mg mL^{-1} *vs.* 5 heating and cooling cycles between 20 and 60 °C.

Preparation of the self-crosslinking nanogels

Upon dispersion of the crosslinked copolymer PEG-*b*-PNSN-*co*-PNAG in water, the nanogel solution was obtained. Transmission electron microscopy (TEM) and dynamic light scattering (DLS) were performed to investigate the nanostructure of the nanogels. PEG-*b*-PNSN-*co*-PNAG upon 10 h of UV-irradiation self-assembles into a spherical structure with a diameter of 40.4 ± 5.6 nm, as observed by TEM (Fig. 5). The size is slightly smaller than that of the nonirradiated micelles (48.5 ± 11.5 nm), possibly because of the more compact structure of the crosslinked micelle. DLS was further used to investigate the size of assemblies. For comparison, both solutions in the presence and absence of UV-irradiation were examined. After constant dilution of the solution, it can be observed that the size of nanogels remains in the range of 20–50 nm after irradiation (Fig. S8a†). In contrast, the size of the assemblies without irradiation decreases significantly with dilution and eventually disappears at a concentration of 0.001 mg ml^{-1}

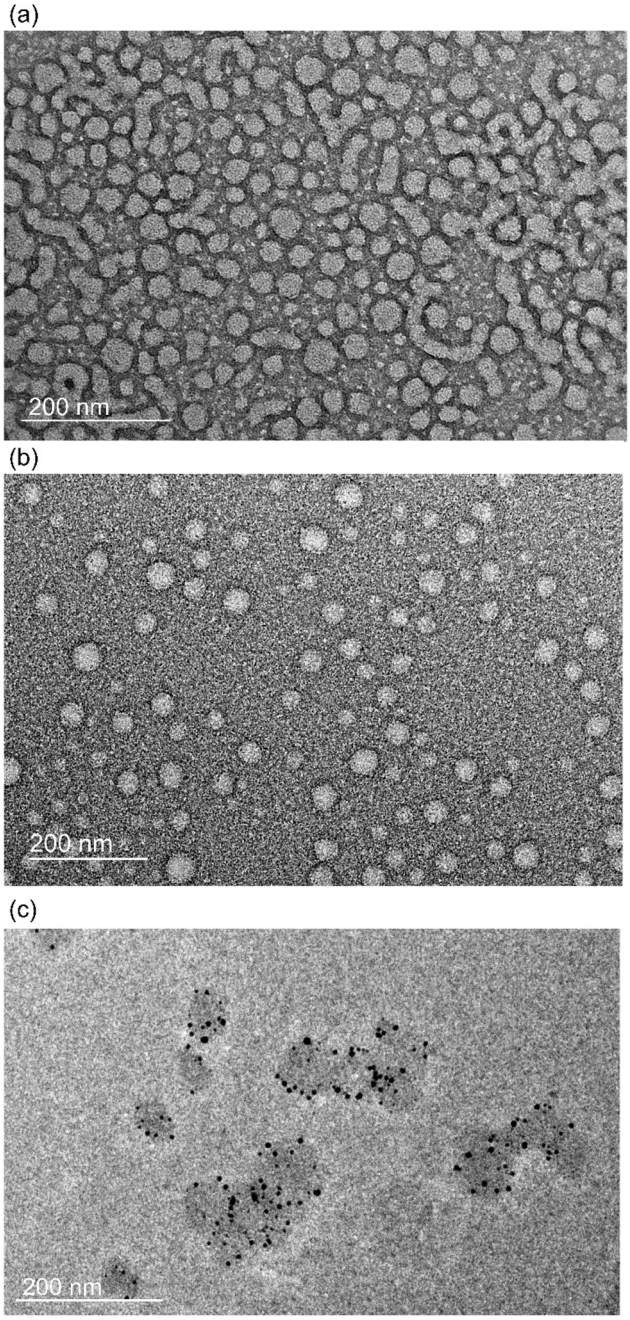

Fig. 5 Transmission electron microscopy (TEM) images of PEG-*b*-PNSN-*co*-PNAG with non-irradiation (a), with 10 h of UV-irradiation (b), and with AuNPs (c) in aqueous solution.

(Fig. S8b†). This indicates that the assemblies dissociate below the critical micelle concentration upon dilution, as the non-covalent hydrophobic interactions dominate the assembly formation.[51] The irradiated system undergoes intra- and intermolecular cross-linking through the thiol–ene reaction, which significantly enhances the stability of the system. Thus, the assemblies remain integrated with dilution, which confirms the crosslinking structure. Considering these advantageous properties, the obtained polypeptoid nanogel is expected to show great potential in nanomedicine and nanotechnology.

AuNP-containing hybrid nanogel

Small-sized gold nanoparticles (AuNPs) show excellent catalytic performance for extensive applications.[59] We prepared the AuNP-containing hybrid nanogel (nanogels@Au) in a one-pot preparation. We first synthesized AuNPs by reduction of $HAuCl_4$ upon UV irradiation in the presence of the photoinitiator I_{2959}.[60] The free thiol groups on the polymers provide opportunities for crosslinking and stabilizing AuNPs during the photolysis of the NB groups. The UV-vis absorption spectra show a similar characteristic absorption of nanogels@Au to traditional AuNPs, suggesting the successful synthesis (Fig. S9†). TEM images show that AuNPs are encapsulated in nanogels (Fig. 5c). The final concentration of Au was determined to be 28.08 g mL^{-1} in the hybrid nanogel solution by inductively coupled plasma emission spectrometry.

The catalytic reduction of 4-nitrophenol (*p*NP) to 4-aminophenol (*p*AP) was used to evaluate the catalytic activity of the polypeptoid–AuNP hybrid nanogel. The process was monitored using a UV-vis spectrometer, where the decreased characteristic absorption peak at 400 nm indicates that *p*NP is gradually reduced to *p*AP (Fig. S10†). As shown in Fig. 6a, *p*NP cannot be reduced in the absence of AuNPs during the experiment period. However, the content of *p*NP starts to significantly decrease within two minutes after the addition of nanogels@Au. Remarkably, the catalytic rate and conversion of nanogels@Au are considerably higher than those of AuNPs at the same concentration of Au. Specifically, all nanogels@Au samples show a reduced content of ~96% from *p*NP to *p*AP within 20 min. In contrast, the free AuNPs exhibit significantly lower efficiency and a higher concentration is required to achieve similar results from nanogels@Au at a low concentration. The plots of $\ln(C_t/C_0)$ *versus* time for both systems are shown in Fig. 6b. The corresponding kinetic reaction rate constants k are determined to be 0.27 min^{-1} and 0.22 min^{-1} for nanogels@Au and free AuNPs, respectively. This suggests that nanogels@Au significantly increases the catalytic activity. The enhancement of the catalytic capability of nanogels@Au is possibly because of the assembly of the AuNPs in nanogels that generates a local domain with amplified activity and the π–π interactions between *p*NP and the nanogels containing the nonphotocleavaged phenyl groups.[54,61]

Hybrid nanogel immobilized with lipase

In spite of many methods being applied to load proteins into nanogels, covalent conjugation is considered to be one of the most effective approaches to form the linkage between proteins and nanogels.[53,62–67] We then conjugated the lipase onto PEG-*b*-PNSN-*co*-PNAG to form a lipase-immobilized hybrid nanogel (nanogels@L) in a one-pot preparation. The thiol-modified lipase is conjugated to the polymer *via* a thiol–ene reaction and simultaneously undergoes the self-crosslinking process (Scheme 1b). 4-Nitrophenyl palmitate (*p*NPP) was selected as a substrate to assess the bioactivity of the hybrid

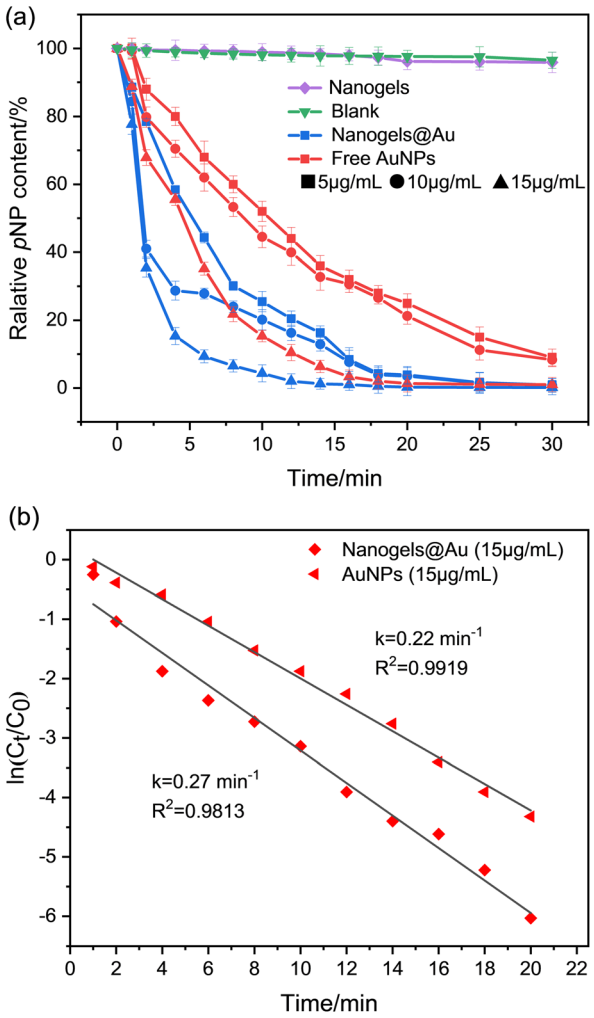

Fig. 6 Catalytic reduction of *p*NP with different additives (a) and the kinetic curve of the catalytic process (b).

nanogels. The catalytic capacities of native lipase and the hybrid nanogels were determined by absorbance of the hydrolysis product of *p*-nitrophenol at λ = 400 nm on a UV-vis spectrometer at 37 °C. In all cases, the hybrid nanogel shows a significantly higher conversion value of >200% compared to native lipase under the same conditions, which is significantly higher than the previously reported results (Fig. 7).[68–73] This is possibly due to the conformational change of lipase that enhances the catalytic activity, consistent with the reported study.[63] Moreover, the hybrid nanogels with lipase at different concentrations show that the hydrolysis efficiency of *p*NPP increases obviously as the polymer concentration increases (Fig. 8). We attribute this to the increased content of polymers that provides more coupling points for the thiol-modified lipase, resulting in higher immobilization efficiency (Fig. 8b). Note that UV irradiation shows trivial influence on the hydrolysis efficiency of lipase (Fig. S11†).

To prepare the stimuli-responsive hybrid nanogels, thermo-responsive *N*-isopropylacrylamide (NIPAM) motifs were also

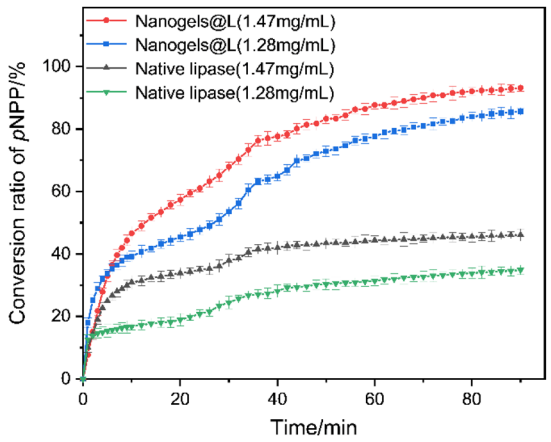

Fig. 7 Conversion of *p*NPP with the hybrid nanogels and native lipase at the same concentration.

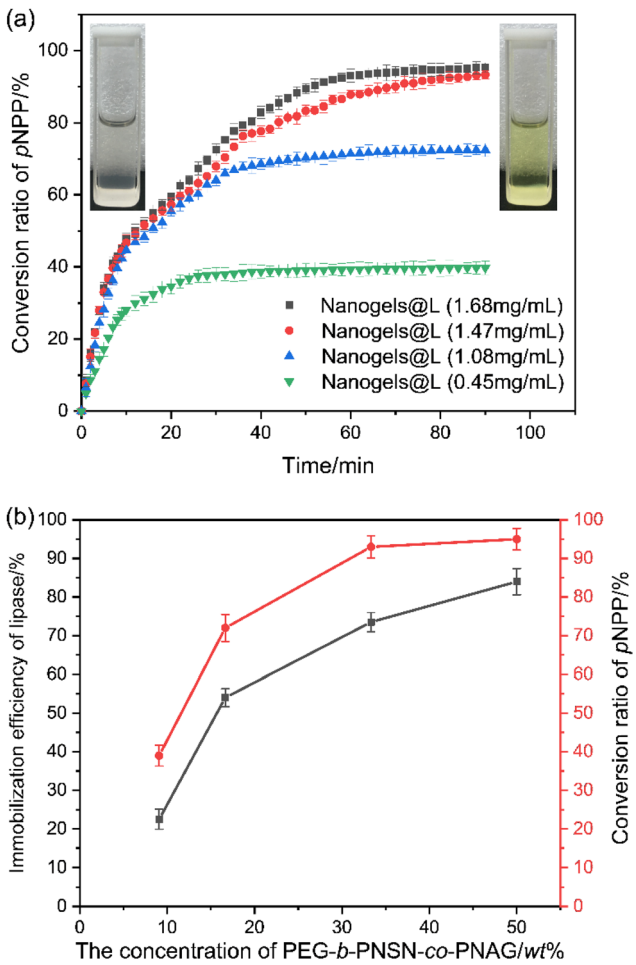

Fig. 8 (a) Catalytic hydrolysis process of *p*NPP by the nanogels with various concentrations. (b) Immobilization efficiency of lipase *versus* the concentration of the polymers.

used in the nanogels (nanogels@NL). The temperature influence on nanogels@NL was evaluated by measuring the catalytic activity of the enzyme at various temperatures.

The residual activity (%) was determined by comparing with that of free lipase at the same concentration. As shown in Fig. 9, with the temperature increasing from 25 °C to 40 °C, both the free lipase and the hybrid nanogels show increased catalytic activity, as it is close to the optimal catalytic temperature of lipase.[73,74] From 25 °C to 30 °C, lower than the LCST of NIPAM-containing polymers, the activity of hybrid nanogels is lower than that of free lipase. In contrast, as the temperature increases to 35 °C and 40 °C, the hybrid nanogels show significantly enhanced efficacy as compared to the native lipase. We attribute this to the fully dissolved polymer chains below the LCST that reduce the effective concentration of the lipase in the hybrid nanogels. As the temperature is higher than the LCST, the molecular chains shrink which enhances the catalytic activity of the enzyme.

The enzyme stability against heat treatment is of great importance. After incubating at different temperatures for 30 min, the residual enzymatic activities of nanogels@NL were assessed and compared with native lipase. Fig. 10 shows that the activities of nanogels@NL are higher than those of the native lipase at both 50 °C and 60 °C, where nanogels@NL exhibits 89.8% and 80.2% of residual enzymatic activities, and 80.2% and 69.7% are observed in the native lipase, respectively. This is possibly due to the immobilization of lipase; the hybrid nanogels can effectively prevent the aggregation of lipase at higher temperatures, thus showing better catalytic activity under the experimental conditions.[63] These results indicate that the obtained hybrid nanogels@NL are potential reservoirs for enzyme immobilization.

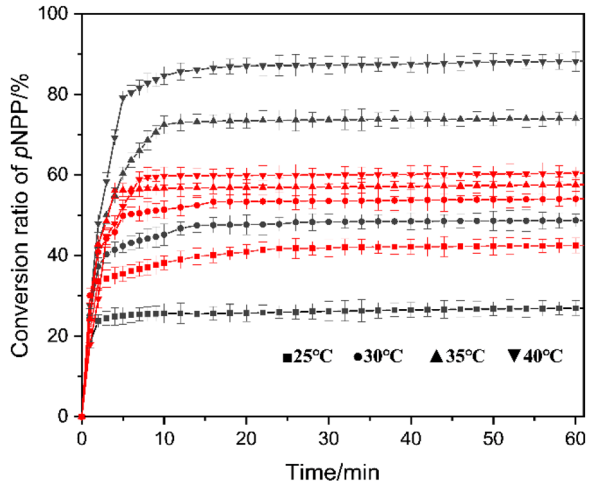

Fig. 9 Hydrolysis of *p*NPP catalysed by nanogels@NL and native lipase at various temperatures. Black line and red line represent the hybrid nanogels and free lipase, respectively.

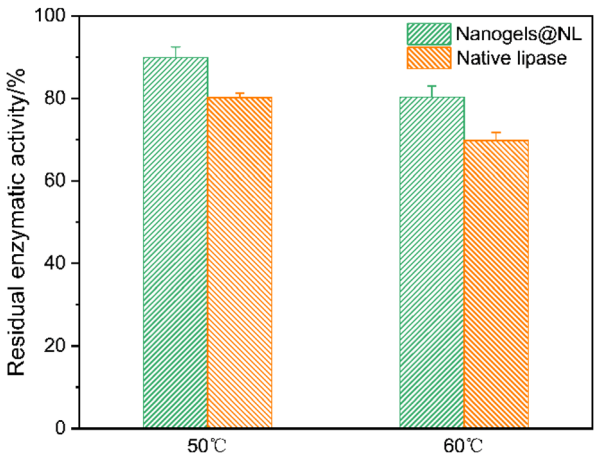

Fig. 10 Enzymatic activity of nanogels@NL and free lipase at different temperatures.

Conclusions

In summary, we prepared a series of polypeptoid derivatives with various side-chain functionalities *via* sequential photocleavage and thiol–ene reactions. All the samples displayed high modification efficiency. In particular, the polypeptoids grafted with thermo-responsive *N*-isopropylacrylamide (NIPAM) motifs exhibit lower critical solution temperature (LCST) properties. Moreover, by incorporation of allyl groups, poly(ethylene glycol)-*b*-poly(*N*-(S-(*o*-nitrobenzyl)-thioethyl) glycine)-*co*-poly(*N*-allyl glycine) (PEG-*b*-PNSN-*co*-PNAG) was prepared, which enabled self-crosslinking to form nanogels for further immobilization of lipase and gold nanoparticles in aqueous solution. Notably, as compared with the free lipase and gold nanoparticles, the obtained hybrid nanogels showed increased catalytic efficiency and adjustable bioactivity. The hybrid nanogel showed a significantly higher conversion of >200% compared to native lipase. In addition, thermo-responsive hybrid nanogels were prepared by including NIPAM motifs and 89.8% of the residual enzymatic activities are retained at 50 °C. This work provides an efficient method to prepare multifunctional peptoid-based bioinspired polymers and offers an efficient nanoscaffold for versatile functionalities.

Author contributions

This manuscript was written through contributions of all authors. All authors have given approval to the final version of the manuscript.

Conflicts of interest

There are no conflicts to declare.

Acknowledgements

This work was supported by the National Natural Science Foundation of China (52073153 and 52273294).

References

1 C. He, S. W. Kim and D. S. Lee, *J. Controlled Release*, 2008, **127**, 189–207.
2 J. F. Mano, *Adv. Eng. Mater.*, 2008, **10**, 515–527.
3 S. Dai, P. Ravi and K. C. Tam, *Soft Matter*, 2009, **5**, 2513–2533.
4 F. Liu and M. W. Urban, *Prog. Polym. Sci.*, 2010, **35**, 3–23.
5 Y. Qiu and K. Park, *Adv. Drug Delivery Rev.*, 2012, **64**, 49–60.
6 F. D. Jochum and P. Theato, *Chem. Soc. Rev.*, 2013, **42**, 7468–7483.
7 D. Roy, W. L. Brooks and B. S. Sumerlin, *Chem. Soc. Rev.*, 2013, **42**, 7214–7243.
8 Y. Shen, X. Fu, W. Fu and Z. Li, *Chem. Soc. Rev.*, 2015, **44**, 612–622.
9 D. He, H. Susanto and M. Ulbricht, *Prog. Polym. Sci.*, 2009, **34**, 62–98.
10 F. Ercole, T. P. Davis and R. A. Evans, *Polym. Chem.*, 2010, **1**, 37–54.
11 J. F. Gohy and Y. Zhao, *Chem. Soc. Rev.*, 2013, **42**, 7117–7129.
12 P. Xiao, J. Zhang, J. Zhao and M. H. Stenzel, *Prog. Polym. Sci.*, 2017, **74**, 1–33.
13 S. Gai, G. Yang, P. Yang, F. He, J. Lin, D. Jin and B. Xing, *Nano Today*, 2018, **19**, 146–187.
14 L. Yang, H. Tang and H. Sun, *Micromachines*, 2018, **9**, 1–18.
15 A. Abdollahi, H. Roghani-Mamaqani, B. Razavi and M. Salami-Kalajahi, *Polym. Chem.*, 2019, **10**, 5686–5720.
16 A. Romano, I. Roppolo, E. Rossegger, S. Schlogl and M. Sangermano, *Materials*, 2020, **13**, 1–26.
17 X. Chang and C. M. Dong, *Biomacromolecules*, 2013, **14**, 3329–3337.
18 P. Li and C.-M. Dong, *ACS Macro Lett.*, 2017, **6**, 292–297.
19 P. Li, J. Zhang and C.-M. Dong, *Polym. Chem.*, 2017, **8**, 7033–7043.
20 S. Ji, L. Xu, X. Fu, J. Sun and Z. Li, *Macromolecules*, 2019, **52**, 4686–4693.
21 G. Liu and C. M. Dong, *Biomacromolecules*, 2012, **13**, 1573–1583.
22 T. Pauloehrl, G. Delaittre, M. Bastmeyer and C. Barner-Kowollik, *Polym. Chem.*, 2012, **3**, 1740–1749.
23 G. Liu, L. Zhou, Y. Guan, Y. Su and C. M. Dong, *Macromol. Rapid Commun.*, 2014, **35**, 1673–1678.
24 X. Wu, L. Zhou, Y. Su and C.-M. Dong, *Polym. Chem.*, 2015, **6**, 6857–6869.
25 X. Wu, L. Zhou, Y. Su and C. M. Dong, *Biomacromolecules*, 2016, **17**, 2489–2501.
26 Y. Gao and C.-M. Dong, *Chin. Chem. Lett.*, 2018, **29**, 927–930.
27 R. D. Murphy, S. Kimmins, A. J. Hibbitts and A. Heise, *Polym. Chem.*, 2019, **10**, 4675–4682.
28 J. Sun and H. Schlaad, *Macromolecules*, 2010, **43**, 4445–4448.
29 L. Chambre, A. Degirmenci, R. Sanyal and A. Sanyal, *Bioconjugate Chem.*, 2018, **29**, 1885–1896.
30 F. Ding, Q. Mou, Y. Ma, G. Pan, Y. Guo, G. Tong, C. H. J. Choi, X. Zhu and C. Zhang, *Angew. Chem., Int. Ed.*, 2018, **57**, 3064–3068.
31 P. Jiang, S. Li, J. Lai, H. Zheng, C. Lin, P. Shi and Y. Wang, *ACS Appl. Mater. Interfaces*, 2017, **9**, 4467–4474.
32 K. Kim, B. Bae, Y. J. Kang, J. M. Nam, S. Kang and J. H. Ryu, *Biomacromolecules*, 2013, **14**, 3515–3522.
33 N. Morimoto, X. Qiu, F. M. Winnik and K. Akiyoshi, *Macromolecules*, 2008, **41**, 5985–5987.
34 B. Aktan, L. Chambre, R. Sanyal and A. Sanyal, *Biomacromolecules*, 2017, **18**, 490–497.
35 R. Kaup, J. B. ten Hove and A. H. Velders, *ACS Nano*, 2021, **15**, 1666–1674.
36 W. Cheng, X. Zeng, H. Chen, Z. Li, W. Zeng, L. Mei and Y. Zhao, *ACS Nano*, 2019, **13**, 8537–8565.
37 A. Yahia-Ammar, D. Sierra, F. Merola, N. Hildebrandt and X. Le Guevel, *ACS Nano*, 2016, **10**, 2591–2599.
38 S. Ghaeini-Hesaroeiye, H. R. Bagtash, S. Boddohi, E. Vasheghani-Farahani and E. Jabbari, *Gels*, 2020, **6**(3), 20.
39 M. Karimi, A. Ghasemi, P. S. Zangabad, R. Rahighi, S. M. M. Basri, H. Mirshekari, M. Amiri, Z. S. Pishabad, A. Aslani, M. Bozorgomid, D. Ghosh, A. Beyzavi, A. Vaseghi, A. R. Aref, L. Haghani, S. Bahrami and M. R. Hamblin, *Chem. Soc. Rev.*, 2016, **45**, 1457–1501.
40 J. Sun and Z. Li, *Acta Polym. Sin.*, 2018, **1**, 1–8.
41 J. Sun and R. N. Zuckermann, *ACS Nano*, 2013, **7**, 4715–4732.
42 N. Gangloff, J. Ulbricht, T. Lorson, H. Schlaad and R. Luxenhofer, *Chem. Rev.*, 2016, **116**, 1753–1802.
43 S. Xuan, C. U. Lee, C. Chen, A. B. Doyle, Y. Zhang, L. Guo, V. T. John, D. Hayes and D. Zhang, *Chem. Mater.*, 2016, **28**, 727–737.
44 R. Hoogenboom and H. Schlaad, *Polym. Chem.*, 2017, **8**, 24–40.
45 A. M. Rosales, R. A. Segalman and R. N. Zuckermann, *Soft Matter*, 2013, **9**, 8400–8414.
46 X. Fu, J. Tian, Z. Li, J. Sun and Z. Li, *Biopolymers*, 2019, **110**, 1–8.
47 C. Xing, Z. Shi, J. Tian, J. Sun and Z. Li, *Biomacromolecules*, 2018, **19**, 2109–2116.
48 J. Tian, J. Sun and Z. Li, *Polymer*, 2018, **138**, 132–138.
49 R. Liu, Z. Shi, J. Sun and Z. Li, *Sci. China: Chem.*, 2018, **61**, 1314–1319.
50 X. Fu, Y. Ma, J. Sun and Z. Li, *RSC Adv.*, 2016, **6**, 70243–70250.
51 J. R. Wei, J. Sun, X. Yang, S. F. Ji, Y. H. Wei and Z. B. Li, *Polym. Chem.*, 2020, **11**, 337–343.
52 X. Yang, Z. Wang and J. Sun, *Polymers*, 2020, **12**, 1–10.
53 J. Liu, X. Ji and H. Zhao, *J. Polym. Sci., Part A: Polym. Chem.*, 2017, **55**, 2047–2052.
54 T. K. Sau and C. J. Murphy, *J. Am. Chem. Soc.*, 2004, **126**, 8648–8649.
55 Z. Shi, Y. Wei, C. Zhu, J. Sun and Z. Li, *Macromolecules*, 2018, **51**, 6344–6351.
56 Y. Ni, J. Sun, Y. Wei, X. Fu, C. Zhu and Z. Li, *Biomacromolecules*, 2017, **18**, 3367–3374.
57 S. H. Lahasky, W. K. Serem, L. Guo, J. C. Garno and D. Zhang, *Macromolecules*, 2011, **44**, 9063–9074.

58 L. W. Xia, R. Xie, X. J. Ju, W. Wang, Q. Chen and L. Y. Chu, *Nat. Commun.*, 2013, **4**, 2226.
59 Y. Dai, T. Ren, Y. Wang and X. Zhang, *Gold Bull.*, 2017, **51**, 21–26.
60 R.-M. Jin, M.-H. Yao, J. Yang, D.-H. Zhao, Y.-D. Zhao and B. Liu, *ACS Sustainable Chem. Eng.*, 2017, **5**, 9841–9847.
61 Y. Zhu, L. Fan, B. Yang and J. Du, *ACS Nano*, 2014, **8**, 5022–5031.
62 N. Morimoto, T. Endo, M. Ohtomi, Y. Iwasaki and K. Akiyoshi, *Macromol. Biosci.*, 2005, **5**, 710–716.
63 S. Sawada and K. Akiyoshi, *Macromol. Biosci.*, 2010, **10**, 353–358.
64 X. Ji, J. Liu, L. Liu and H. Zhao, *Colloids Surf., B*, 2016, **148**, 41–48.
65 Q. Tao, A. Li, Z. Zhang, R. Ma and L. Shi, *ACS Biomater. Sci. Eng.*, 2017, **3**, 3141–3145.
66 Q. Wu, Z. He, X. Wang, Q. Zhang, Q. Wei, S. Ma, C. Ma, J. Li and Q. Wang, *Nat. Commun.*, 2019, **10**, 240.
67 E. W. McConnell, A. L. Smythers and L. M. Hicks, *J. Am. Soc. Mass Spectrom.*, 2020, **31**, 1697–1705.
68 J. Zhang, X. Chen, P. Lv, W. Luo, Z. Wang, J. Xu and Z. Wang, *Fuel*, 2021, **304**, 121594.
69 A. Nuraliyah, M. S. Perdani, D. N. Putri, M. Sahlan, A. Wijanarko and H. Hermansyah, *Front. Energy Res.*, 2021, **9**, 616945.
70 S. S. Nadar and V. K. Rathod, *Int. J. Biol. Macromol.*, 2020, **152**, 1108–1112.
71 T. Guan, B. Liu, R. Wang, Y. Huang, J. Luo and Y. Li, *Food Hydrocolloids*, 2021, **116**, 106651.
72 F. O. Rottke, M. V. Heyne and S. Reinicke, *Chem. Commun.*, 2020, **56**, 2459–2462.
73 N. Rueda, J. C. Dos Santos, R. Torres, C. Ortiz, O. Barbosa and R. Fernandez-Lafuente, *Methods Enzymol.*, 2016, **571**, 73–85.
74 C. Mateo, J. M. Palomo, G. Fernandez-Lorente, J. M. Guisan and R. Fernandez-Lafuente, *Enzyme Microb. Technol.*, 2007, **40**, 1451–1463.

